

The YNEV stellar evolution and oscillation code *

Qian-Sheng Zhang

Yunnan Observatories, Chinese Academy of Sciences, Kunming 650011, China; zqs@ynao.ac.cn
Key Laboratory for the Structure and Evolution of Celestial Objects, Chinese Academy of
Sciences, Kunming 650011, China

Received 2014 February 18; accepted 2014 June 26

Abstract We have developed a new stellar evolution and oscillation code YNEV, which calculates the structures and evolutions of stars, taking into account hydrogen and helium burning. A nonlocal turbulent convection theory and an updated overshoot mixing model are optional in this code. The YNEV code can evolve low- and intermediate-mass stars from the pre-main sequence to a thermally pulsing asymptotic branch giant or white dwarf. The YNEV oscillation code calculates the eigenfrequencies and eigenfunctions of the adiabatic oscillations for a given stellar structure. The input physics and numerical scheme adopted in the code are introduced. Examples of solar models, stellar evolutionary tracks of low- and intermediate-mass stars with different convection theories (i.e. mixing-length theory and nonlocal turbulent convection theory), and stellar oscillations are shown.

Key words: stars — stellar structure — stellar evolution — stellar oscillations

1 INTRODUCTION

We have developed a new stellar evolution and oscillation code named YunNan EVolution code (YNEV). This evolution code calculates the structures and evolutions of stars, taking into account hydrogen and helium burning. A feature of this code is that a nonlocal turbulent convection theory and an updated overshoot mixing model are optional to deal with stellar turbulent convection. This evolution code can evolve a single low- or intermediate-mass star with spherical symmetry from the pre-main sequence (PMS) stage with a center temperature $T_C = 10^5$ K to a thermally pulsing asymptotic branch giant (TP-AGB) (for intermediate-mass stars) or white dwarf (for low-mass stars). The accessorial oscillation code calculates the eigenfrequencies and eigenfunctions of adiabatic oscillations for a given stellar structure. This paper introduces the input physics and the numerical scheme adopted in the code and shows examples of solar models, stellar evolutionary tracks and stellar oscillations.

The contents of this paper are as follows: the physics involved in the YNEV code and their treatments are described in Section 2, the numerical calculations and the time/space step setting are introduced in Section 3, the generations of initial stellar models are introduced in Section 4, examples of stellar structures and evolutions, and stellar oscillations are shown in Section 5, and possible improvements are discussed in Section 6.

* Supported by the National Natural Science Foundation of China.

2 INPUT PHYSICS

2.1 Equation of State

The equation of state (EOS) part of the YNEV code calculates thermal functions of pressure P , $(\partial \ln P / \partial \ln T)_\rho$, $(\partial \ln P / \partial \ln \rho)_T$, adiabatic temperature gradient $(\partial \ln T / \partial \ln P)_S$ and specific heat c_P for input density ρ , temperature T and chemical abundance X_i .

In the low T (default of $\lg T < 8.2$) and low Z (default of $Z < 0.045$) regime, we use the EOS2005 tables (Rogers & Nayfonov 2002) to interpolate the thermal functions of gas, and then modify the thermal functions by taking into account the contribution of the radiative field which is assumed to be in local thermodynamic equilibrium with the gas. In the calculations of thermal functions for gas, we adopt a bicubic interpolation on ρ and T in order to obtain smooth (such that first-order derivatives exist) thermal functions, and use linear interpolations on hydrogen abundance X and Z (for Z , quadratic interpolation between three tables with different metallicity values is optional and this is usually used in solar models).

In the high T (default of $\lg T > 8.3$) or high Z (default of $Z > 0.05$) regime, we assume there is an ideal gas mixture comprised of ions, electrons, positrons and the radiative field. The thermal functions of the ideal gas mixture can be solved by using statistical physics (see, e.g., Timmes & Arnett 1999). In order to reduce the time costs in the calculations of thermal functions for electrons and positrons, we interpolate them from a table calculated offline. The table lists thermal functions of electrons and positrons with different values for rest electron number density ρ_E (in mol cm^{-3}) and temperature T . In the calculations used for constructing the table, Aparicio's (1998) scheme is adopted to calculate the integral of the Fermi functions.

In the connecting region between the above parts, we interpolate thermal functions from the two schemes above as follows. For a thermal function, say A , we denote the value of A calculated using the first scheme to be A_1 and that using the second scheme to be A_2 . We calculate the final result of A by using the interpolation:

$$\begin{aligned} A &= aA_1 + (1 - a)A_2, \\ a &= f(\lg T, 8.2, 8.3)f(Z, 0.045, 0.05), \\ f(x, x_1, x_2) &\equiv \frac{1}{2} \left\{ 1 - \sin \left\{ \left\{ \max \left[0, \min \left(1, \frac{x - x_1}{x_2 - x_1} \right) \right] - \frac{1}{2} \right\} \pi \right\} \right\}. \end{aligned} \quad (1)$$

It is obvious that the interpolation leads to a smooth thermal function denoted by A .

2.2 Opacity

There is a part of YNEV that calculates opacity for input density ρ , temperature T and chemical abundance X_i . Similar to the EOS, the bicubic interpolation on ρ and T and linear interpolations of hydrogen abundance X and Z (for Z , quadratic interpolation is optional) are performed. The opacity tables are the same as those used in MESA (Paxton et al. 2011). For the electron conduction opacity, Cassisi et al. (2007), Iben (1975) and Yakovlev & Urpin (1980) are used. For the radiative opacity, the OPAL tables with fixed metallicity and enhanced CO (Iglesias & Rogers 1996) are used. The OP tables (Seaton 2005) and the F05 low-temperature tables (Ferguson et al. 2005) are also employed.

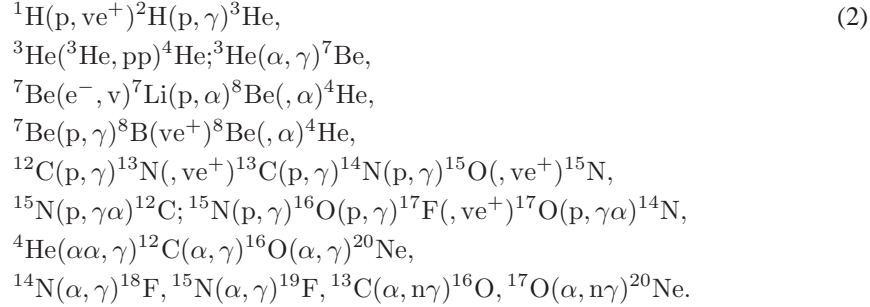
The choice of using tables with fixed metallicity or with enhanced CO is based on the input chemical abundance X_i . Tables with fixed metallicity are adopted in the case of $Z \leq 0.045$ and tables with enhanced CO are adopted in the case of $Z \geq 0.05$. A smooth interpolation similar to the EOS is used when $0.045 < Z < 0.05$. Since the YNEV code can be used for stars with initial $Z < 0.04$ (higher Z is not supported by the EOS tables, and we do not attempt to use the ideal gas mixture model in the envelope of a star), this scheme is in general reasonable. An inconsistency occurs at the start of helium burning, where tables with enhanced CO should be used but tables with

fixed metallicity are actually implemented. This should not lead to unacceptable results, since the duration from the helium ignition to $Z = 0.05$ is not long.

2.3 Nuclear Reaction

In the YNEV stellar evolution code, we trace the evolution of the following elements: ^1H , ^2H , ^3He , ^4He , ^7Li , ^{12}C , ^{13}C , ^{14}N , ^{15}N , ^{16}O and ^{17}O .

The hydrogen and helium burnings (p-p chains, CNO cycles, 3α , 4α and 5α reactions) are taken into account:



The basic rates of all reactions above are based on Angulo et al. (1999), except for the β -decay of ^7Be , which is based on Caughlan & Fowler (1988). The electron screening factors are based on Salpeter (1954) (for weak screening) and Dewitt et al. (1973) (for intermediate or strong screening) with a smooth interpolation. The neutrino energy loss rates are calculated by using a public code by Itoh et al. (1996). In the calculation of chemical evolution due to nuclear reactions, we use an implicit scheme to work out the nuclear reaction networks, and the abundance of ^7Be is assumed to be in equilibrium. In the fully mixed burning zone (e.g. convective burning core), nuclear rates are integrated over the whole zone to calculate variations in the average chemical abundance. The initial metal composition can be set to values given by Grevesse & Noels (1993) (GN93), Grevesse & Sauval (1998) (GS98) or Asplund et al. (2009) (AGSS09). The initial abundance of isotopes D (i.e. ^2H), ^3He , ^7Li , ^{13}C , ^{15}N and ^{17}O are based on AGSS09.

2.4 Convection

Convection in the stellar interior plays an important role because this convection leads to entropy and chemical mixing which dominates the stellar structure and evolution. Unfortunately, properties associated with convection are still not very clear. At present, a local convection theory named Mixing-Length Theory (MLT) (Böhm-Vitense 1958) is widely used in modeling stars. Although MLT has some significant shortcomings (for example, it is a phenomenological theory, it is unable to be used in the study of convective overshoot and it describes stellar turbulence as a single length scale), it is very convenient to implement in code. More reasonable theories of stellar convection are the Turbulent Convection Models (TCMs) (e.g., Xiong 1981; Xiong et al. 1997; Canuto 1997, 2011; Canuto & Dubovikov 1998; Deng et al. 2006; Li & Yang 2007; Li 2012) which are based on equations from fluid dynamics. The TCMs are capable of studying the overshoot and show results that are consistent with helioseismology (Christensen-Dalsgaard et al. 2011). On the other hand, on a large scale, the results of the MLT theory are similar to those of TCM except for the case of a convective envelope and a convective stable region. For convection zones in the stellar interior, both MLT and TCM show efficient entropy and chemical mixing so that the temperature gradient is almost adiabatic and chemical elements are fully mixed.

In the standard version of the YNEV code, the MLT is still adopted to deal with convective entropy transport. Also, the convective unstable zone (i.e. the convection zone as determined by the

Schwarzschild criterion) is artificially fully mixed and convective overshoot can be taken into account in the traditional way in that the artificially fully mixed region is extended by $l_{OV} = \alpha_{OV} H_P$, where H_P is the pressure scale height and α_{OV} is a parameter. In the helium burning phase, the induced semiconvection outside the convective core is implemented (Castellani et al. 1985). The temperature gradient ∇ determined by the standard MLT theory is calculated as follows (which may not have appeared before but is equivalent to other forms of the standard MLT theory)

$$f^3 + af^2 + (b-a)f - b = 0, \quad (3)$$

where

$$\begin{aligned} f &= \frac{\nabla - \nabla_{ad}}{\nabla_R - \nabla_{ad}}, \\ a &= \frac{23}{4}K^{-1}; \quad b = \left(1 + \frac{729}{64}K^{-1}\right)K^{-1}, \\ K &= \frac{1}{32} \left[\left(\frac{\alpha \rho c_p l}{\lambda} \right)^2 g \delta H_P (\nabla_R - \nabla_{ad}) \right], \end{aligned} \quad (4)$$

and $l = \alpha H_P$ in which l and α are the mixing length and the MLT parameter respectively. A table of the roots f within an accuracy of 10^{-13} with different values of K in the range $-5 \leq \lg K \leq 40$ was calculated offline. When we need to solve the MLT, the table is read to get a good initial value of f for input K , which converges with high accuracy after a few Newton iterations. Outside the range $-5 \leq \lg K \leq 40$, the following approximate solutions within the accuracy of f being 10^{-12} are used

$$\begin{aligned} f &= 1 - \frac{64}{729}K^2, \quad \lg K < -5; \\ f &= K^{-\frac{1}{3}}, \quad \lg K > 40. \end{aligned} \quad (5)$$

It is not difficult to find those approximate solutions based on the behavior described by Equation (3) as $K \rightarrow 0$ or $K \rightarrow +\infty$.

In a beta version of the YNEV code, the TCM developed by Li & Yang (2007) can be used to replace the MLT to study convective entropy transport, and the turbulent convective mixing model developed by Zhang (2013) can be used to study convective overshoot mixing.

2.5 Diffusion

The particle diffusion and gravitational settling, which are optional in the code, are calculated by solving Burger's equations with diffusion velocities/coefficients given by Thoul et al. (1994). The elements are assumed to be fully ionized. The electrons are included. By default, ^1H , ^3He , ^4He , ^{12}C , ^{13}C , ^{14}N and ^{16}O are taken into account and other elements are assumed to be ^{20}Ne .

2.6 Atmosphere

Boundary conditions for the atmosphere are based on the definition of effective temperature and the implementation of the adopted $T - \tau$ relation $T = T(\tau)$. In the YNEV code, the outer boundary of stellar structure equations is set to be the location where $T = T_{\text{eff}}$. The definition of effective temperature gives a boundary condition $L_S = 4\pi r_S^2 \sigma T_S^4$. Another boundary condition is based on the integral of the differential equation describing the atmosphere (assumed to be homogeneous)

$$\frac{d \ln \rho}{d\tau} = \delta \left[\frac{g}{P\kappa} \left(\frac{\partial \ln T}{\partial \ln P} \right)_\rho - \frac{d \ln T}{d\tau} \right], \quad (6)$$

where $\delta = -(\partial \ln \rho / \partial \ln T)_P$ and $g = GM/R^2$; g is assumed to be a constant in the atmosphere. The region where this differential equation can be applied is from $\tau = 0$ to $\tau = \tau_S$ where τ_S is defined by $(T_{\text{eff}} =)T_S = T(\tau_S)$, and we adopt the initial condition $\rho_{\tau=0} = 10^{-10}$. We set the initial condition of the equation above as $\rho_{\tau=0} = 10^{-10}$ by default. The second-order Runge-Kutta method is adopted in the numerical solution. The solution gives the value of density at the surface ρ_S . $d \ln T / d\tau$ and the value of τ_S are determined by the adopted $T - \tau$ relation. In the YNEV code, there are two optional $T - \tau$ relations: the Eddington gray model and Krishna Swamy's (1966) $T - \tau$ relation.

2.7 Mass Loss

The mass loss is implemented in the YNEV code by ejecting the stellar outer envelope with the mass $M_{\text{env}} = -dM/dt \cdot \Delta t$ where dM/dt is the mass loss rate and Δt is the time step between the current stellar model and the previous one. There are three options for the mass loss rate: Reimers (1975), Waldron (1985) and de Jager et al. (1988). It is not difficult to implement other expressions for the mass loss rate.

3 NUMERICAL CALCULATION

3.1 Numerical Scheme

The code assumes that the star is one-dimensional and in hydrostatic equilibrium, and ignores the effects of rotation. The evolution of the element abundances in the stellar interior and the stellar structure equations are solved alternatively. The evolution of the element abundances is calculated based on the previous stellar structure, then the new structure is determined by the updated element abundance profile. Although this scheme may lead to problems with self consistency, the errors are small in most cases since the time step is not very large.

The stellar structure equations are written in the form as follows:

$$\frac{d \lg P}{dq} + \frac{Mm(1-m)}{\ln 10} \frac{g}{4\pi r^2 P} = 0, \quad (7)$$

$$\frac{d \lg T}{dq} + \frac{Mm(1-m)}{\ln 10} \frac{g \nabla}{4\pi r^2 P} = 0, \quad (8)$$

$$\frac{d \lg r}{dq} - \frac{Mm(1-m)}{\ln 10} \frac{1}{4\pi r^3 \rho} = 0, \quad (9)$$

$$\frac{dl_r}{dq} - \frac{Mm(1-m)}{L_0} \left[\varepsilon_N - \varepsilon_\nu - \left(c_P \frac{\partial T}{\partial t} - \frac{\delta}{\rho} \frac{\partial P}{\partial t} \right) \right] = 0, \quad (10)$$

where the independent variable $q = \ln[m/(m-1)]$, $m = M_r/M$ is the mass fraction, $l_r = L_r/L_0$ is dimensionless luminosity, and $L_0 = \max(L_r)$ is the maximum value of luminosity in the stellar interior. ∇ is the temperature gradient determined by convection theory, e.g. for the MLT theory, and ∇ is calculated by using Equations (3) and (5). The boundary conditions are as follows: for the inner boundary where $r = r_1$

$$r_1^3 = \frac{3m_1}{4\pi\rho_1}, \quad (11)$$

and

$$l_{r,1} = \frac{m_1}{L_0} \left[\varepsilon_N - \varepsilon_\nu - \left(c_P \frac{\partial T}{\partial t} - \frac{\delta}{\rho} \frac{\partial P}{\partial t} \right) \right]_1, \quad (12)$$

and for the outer boundary where $r = r_N$

$$l_{r,N}L_0 = 4\pi r_N^2 \sigma T_N^4; \quad (T_N = T_{\text{eff}}), \quad (13)$$

and

$$\rho_N = \rho_S, \quad (14)$$

where ρ_S is determined by integrating the differential equation representing the atmosphere described in Section 2.6 from $\tau = 0$ to $\tau = \tau_S$.

The chemical evolution equations in the stellar interior are in general given by the diffusion equation

$$\frac{\partial \mathbf{X}}{\partial t} + b \frac{\partial(a\mathbf{F})}{\partial q} = b \frac{\partial}{\partial q} \left(a^2 b \mathbf{D} \frac{\partial \mathbf{X}}{\partial q} \right) + \mathbf{R}; \quad \left\{ a = \frac{dm}{dr}, b = \frac{dq}{dm} \right\}, \quad (15)$$

where \mathbf{X} is the chemical abundance vector, \mathbf{F} is the flux vector, \mathbf{D} is the matrix of diffusion coefficients, and \mathbf{R} is a vector of the nuclear reaction rates. When settling is taken into account, F and D are calculated based on Thoul et al. (1994). The convective/overshoot mixing can be represented by adding a diffusion coefficient to the diagonal components in D . This equation can be rewritten as two first-order equations by defining \mathbf{W} as the total diffusion flux vector:

$$b \frac{\partial(a\mathbf{W})}{\partial q} - \left(\mathbf{R} - \frac{\partial \mathbf{X}}{\partial t} \right) = 0, \quad (16)$$

$$abD \frac{\partial \mathbf{X}}{\partial q} - (\mathbf{F} - \mathbf{W}) = 0. \quad (17)$$

The boundary conditions for the diffusion equations are

$$\mathbf{W} = 0, \quad (18)$$

at the center and the stellar surface.

The radial part of the stellar adiabatic oscillation equation is a linear differential equation

$$\frac{\partial \mathbf{J}}{\partial \ln r} - A(r, \omega) \mathbf{J} = 0, \quad (19)$$

where $\mathbf{J} = (\xi_r, P', \Phi', g')^T$ is the vector determining the properties of stellar oscillations, \mathbf{A} is the coefficient matrix of the oscillation equation, and ω is the frequency. The elements of matrix \mathbf{A} can be found in literature about stellar oscillations. Two boundary conditions are at the center and the other two boundary conditions are at the surface. Four boundary conditions are all linear and homogeneous.

The stellar structure Equations (7)–(14), the diffusion Equations (16)–(18) and the stellar adiabatic oscillation Equation (19) are all first-order equations with two points that act as boundary conditions. We use the Newton iterations (linearization) method to obtain solutions with the two points as boundary conditions (7)–(14) and (16)–(18). The implicit discretization is adopted for the time derivative in Equations (10), (16) and (17). Equation (19) and its boundary conditions are already linear. The general form of those problems is

$$H \left(\frac{\partial U}{\partial q}, U, q \right) = 0, \quad (20)$$

with the boundary conditions at q_1 and q_N being

$$B(U_1, q_1) = 0, \quad (21)$$

$$C(U_N, q_N) = 0, \quad (22)$$

where q is the independent variable, \mathbf{U} is the vector of dependent variables with n elements, elements in vectors \mathbf{H} (including n elements), B (including n_1 elements), C (including $n_2 = n - n_1$ elements) are determined by the differential equations and equations of the boundary conditions. The two point second order discretization is adopted. For the diffusion equation, we adopted the conservation form, in which the flux and the chemical abundance are not represented by the same mesh points, to ensure a correct flux, i.e. we set W_k to be W at the middle point between mesh point k and $k + 1$. In general, the first-order equation between mesh point k and $k + 1$ is as follows

$$H_k = H_k(U_k, U_{k+1}) = 0; \quad k = 1, 2, \dots, N - 2, N - 1. \quad (23)$$

We use the method of Newton iterations to solve these equations on all mesh points. Expanding $H_k(U_k, U_{k+1})$ around the initial solution $U^{(i)}_k$ (for the stellar structure equations and the diffusion equations, which are time-dependent, the initial solution $U^{(0)}$ is set as the values in the previous model, and for stellar oscillations, the initial solution is $U^{(0)} = O$) and ignoring higher order term, we found

$$\frac{\partial H_k}{\partial U_k} \Delta U_k + \frac{\partial H_k}{\partial U_{k+1}} \Delta U_{k+1} = -H_k(U^{(i)}_k, U^{(i)}_{k+1}); \quad k = 1, 2, \dots, N - 2, N - 1, \quad (24)$$

where $\partial H_k / \partial U_k$ and $\partial H_k / \partial U_{k+1}$ are Jacobi matrices. A revised solution is

$$U^{(i+1)}_k = U^{(i)}_k + \Delta U_k. \quad (25)$$

For the boundary conditions, similar results are

$$\frac{\partial B}{\partial U_1} \Delta U_1 = -B(U^{(i)}_1), \quad (26)$$

$$\frac{\partial C}{\partial U_N} \Delta U_N = -C(U^{(i)}_N). \quad (27)$$

Equations (24), (26) and (27) are the complete equations for calculating the corrections ΔU_k . Those equations are equivalent to a linear equation with a huge coefficient matrix with only the elements at/near the diagonal being nonzero. It is not difficult to solve these equations by using the method of forward eliminations and backward recursions. When the corrections are not small enough, the elements in vector \mathbf{H} are therefore not close enough to zero. We then repeat this process until the corrections are in the allowed range of errors. Typically, we set the accuracies as $\max(|\delta \lg \rho|, |\delta \lg T|, |\delta \lg r|, |\delta l_r|) < 10^{-6}$ in the stellar structure equations, and $|\delta X(^1\text{H})| < 10^{-8}$, $|\delta X(^4\text{He})| < 10^{-8}$ and $|\delta X_i / \max(10^{-10}, X_i)| < 10^{-8}$ for other chemical elements in the chemical evolution equation. The oscillation equation is already linear, and it is equivalent to Equations (24)–(27) with $U^{(0)} = O$. We only need to solve the linear equations once.

In scanning the eigenfrequencies in the oscillation equation, we define the discriminant $V(\omega)$ as the determinant of the coefficient matrix of the equation on an arbitrary mesh point k_0 (by default $k_0 = N$)

$$P_{k_0} \Delta U_{k_0} = Q_{k_0}; \quad V(\omega) = \text{Det}(P_{k_0}), \quad (28)$$

where the coefficient matrix P_{k_0} and the vector Q_{k_0} can be worked out in the process of forward eliminations and backward recursions. ω is an eigenfrequency when $V(\omega) = 0$, since the homogeneous equation only has nonzero solutions if the coefficient matrix has a singularity. This definition ensures the continuity of the discriminant $V(\omega)$ and makes it convenient to scan for eigenfrequencies. In solving for eigenfunctions U of a validated eigenfrequency ω_i , we use an inhomogeneous boundary condition (e.g. $\xi_r = 1$) to replace a homogeneous boundary condition in order to eliminate the singularity in the coefficient matrix.

3.2 Numerical Scheme: Implementing the Turbulent Convection Model

In a beta version of the YNEV evolution code, the TCM developed by Li & Yang (2007) can replace the MLT theory and be used to calculate variables associated with TCM. The equations describing TCM are as follows:

$$\frac{2}{\rho r^2} \frac{\partial}{\partial r} \left(\rho r^2 C_s k_r \tau \frac{\partial k_r}{\partial r} \right) = \frac{1}{3} k \tau^{-1} - \frac{\delta g}{T} \overline{u_r' T'} + C_k \tau^{-1} \left(k_r - \frac{k}{3} \right), \quad (29)$$

$$\frac{2}{\rho r^2} \frac{\partial}{\partial r} \left(\rho r^2 C_s k_r \tau \frac{\partial k}{\partial r} \right) = k \tau^{-1} - \frac{\delta g}{T} \overline{u_r' T'}, \quad (30)$$

$$\frac{4}{\rho r^2} \frac{\partial}{\partial r} \left(\rho r^2 C_{t1} k_r \tau \frac{\partial \overline{u_r' T'}}{\partial r} \right) = -\frac{\delta g}{T} \overline{T' T'} - 2k_r \frac{T}{H_P} (\nabla - \nabla_{\text{ad}}) + C_t (1 + P_e^{-1}) \tau^{-1} \overline{u_r' T'}, \quad (31)$$

$$\frac{1}{\rho r^2} \frac{\partial}{\partial r} \left(\rho r^2 C_{e1} k_r \tau \frac{\partial \overline{T' T'}}{\partial r} \right) = -\overline{u_r' T'} \frac{T}{H_P} (\nabla - \nabla_{\text{ad}}) + C_e (1 + P_e^{-1}) \tau^{-1} \overline{T' T'}, \quad (32)$$

where $k_r = \overline{u_r' u_r'}/2$ is the radial turbulent kinetic energy, k is the turbulent kinetic energy, $\overline{u_r' T'}$ describes the convective heat flux, $\overline{T' T'}$ is the temperature variance, $\tau = k/\varepsilon$ is the dissipation timescale with the turbulent dissipation rate $\varepsilon = k^{3/2}/l$ and $l = \alpha_{\text{TCM}} H_P$, and $P_e = lk^{1/2}/D_R$ is the Péclet number with radiative diffusion coefficient $D_R = \lambda/(\rho c_P)$. C_s , C_{t1} and C_{e1} are dimensionless diffusion coefficients, α_{TCM} , C_t and C_e are dimensionless dissipation coefficients, and C_k is a parameter that dominates the rate of k_r/k .

The default values for the parameters in the TCM are as follows (Zhang & Li 2012; Zhang 2012): $C_s = 0.08$, $C_t = 7.5$, $C_e = 0.2$, $C_k = 2.5$, $C_{t1} = 0.02$ or 0, and $C_{e1} = 0.02$ or 0. The turbulent kinetic dissipation parameter $\alpha_{\text{TCM}} = 0.8$ is based on the solar calibration with Eddington's gray atmosphere model, or $\alpha_{\text{TCM}} = 1.0$ for Krishna Swamy's (1966) atmosphere model. Solar calibrations for different compositions show $\alpha = (2.1 \sim 2.2)\alpha_{\text{TCM}}$.

We solve the stellar structure equations and the TCM equations alternately to find the solution satisfying both equations. The TCM equations are solved by using an iterative method based on the multigrid method. In numerically solving the TCM equations, the variables (except for the temperature gradient ∇) are based on the current stellar structure. The following equation is substituted into the TCM equations for the temperature gradient ∇

$$\nabla = \nabla_{\text{R,therm}} - \frac{H_P}{T} \frac{\rho c_P \overline{u_r' T'}}{\lambda}, \quad (33)$$

where $\nabla_{\text{R,therm}}$ is the radiative temperature gradient for thermal energy flux (Zhang 2014)

$$\nabla_{\text{R,therm}} = \nabla_R - \frac{H_P}{T} \frac{F_K}{\lambda}, \quad (34)$$

and F_K is the turbulent kinetic energy flux calculated as follows

$$F_K = -2C_s \rho k_r \tau \frac{\partial k}{\partial r}. \quad (35)$$

In solving the TCM equations, $\nabla_{\text{R,therm}}$ is determined by the current stellar structure and the previous turbulent kinetic energy flux.

The steps for implementing TCM in the code have been described by Zhang (2012):

- (1) Solve the TCM equations based on the current stellar structure and previous turbulent kinetic energy flux. Calculate the temperature gradient ∇ at all mesh points according to Equation (33).
- (2) Solve the localized TCM in which the diffusion terms are ignored. Calculate the corresponding temperature gradient ∇_L at all mesh points.
- (3) Calculate the ratio $\eta = \nabla/\nabla_L$ at all mesh points. Calculate a relaxed $\eta' = \eta'_{\text{pre}} + \xi(\eta - \eta'_{\text{pre}})$, where the subscript “pre” means previous values. The relaxation parameter ξ is 0.618 by default.
- (4) Solve the stellar structure equations in which the temperature gradient is calculated as $\nabla = \eta'\nabla_L$ and update the stellar structure. ∇_L is calculated by the localized TCM when solving the stellar structure equations.
- (5) Check the differences $|\eta - \eta'|$ and $|\eta - \eta_{\text{pre}}|$. The calculations are thought to converge if both differences are less than the required accuracy (10^{-3} by default) at all mesh points; otherwise, return to step 1.

Although the relaxation improves the numerical stability and ensures that the scheme works in most cases of stellar evolutions, it should be mentioned that this implementation of TCM still does not work in some cases. There are still some numerical problems when implementing TCM.

When the TCM is adopted, the updated overshoot mixing model by Zhang (2013) is also adopted in solving the stellar chemical evolution. The diffusion coefficient for mixing in the overshoot region in this model is as follows

$$D_{\text{OV}} = C_{\text{OV}} \frac{\varepsilon}{N_{\text{turb}}^2}, \quad (36)$$

where N_{turb}^2 is calculated as

$$N_{\text{turb}}^2 = -\frac{\delta g}{H_P} \left[\nabla - \nabla_{\text{ad}} - C_1 C_A \sum_{k=1}^M \left(\frac{\partial \ln T}{\partial X_k} \right)_{P, \rho, X - \{X_k\}} \frac{dX_k}{d \ln P} \right], \quad (37)$$

where $C_A = C_e + C_{\text{OV}}$ and, according to Canuto (2011), $C_1 = \sigma_t = 0.72$. The turbulent dissipation rate ε is calculated by using the TCM. It is optional to use the exact representation of the diffusion coefficient (see Zhang 2013, equation (26)), but there is no obvious difference. The only parameter, i.e. the dimensionless diffusion coefficient C_{OV} , is suggested to be $C_{\text{OV}} \sim 10^{-3}$ based on tests of the solar model and the restriction of the classical overshoot length being less than $0.4H_P$ (Zhang 2013), and the calibrations on effective temperatures and radii for low-mass eclipsing binary stars (Meng & Zhang 2014).

3.3 Time Step

In the normal case, the time step in the calculations of stellar evolution depends on the following factors: the maximum correction from the Newton iterations, the variations of ^1H and ^4He abundance in the center, the ratio of burned ^1H in the previous time step to ^1H abundance in the center, the ratio of burned ^1H (and ^4He) in the previous time step to ^1H (and ^4He) abundance in burning shells, the ratio of burned minor elements (D, ^3He , ^7Li and ^{12}C) in the previous time step to their abundances in the center during the PMS stage, and variations of $\lg T_{\text{eff}}$ and $\lg L$ between the previous two stellar models.

When a solution for stellar structure converges in the Newton iterations, the time step for the next stellar model is estimated by taking into account those factors. In the next calculation of the stellar structure, if there is no convergence, the time step is reduced and calculations are redone. If there is still no convergence after reducing the time step and re-calculating many times (50 by default), the code checks whether helium flashes occur in the stellar model. In the case of a helium flash, we do not attempt to trace the changes in stellar structure and let the star jump to the zero age horizontal branch (ZAHB) model. In the case of no helium flash, the code stops.

3.4 Space Step

The mesh points in the calculation of stellar structure are controlled by the differences in $\lg \rho$, $\lg T$, r/R , L_r/L_{\max} , $\lg \tau$, $\ln[M_r/(M - M_r)]$ (the independent variable) and X_i (chemical abundance of all elements) between two adjacent grids. Near the Schwarzschild convective boundaries and the boundaries of artificially fully mixed regions, the density of mesh points is enhanced to be 5–10 times the normal case. This is designed to ensure accuracy in the location of convective boundaries and the boundaries of fully mixed regions, which may sensitively affect the outcome of stellar evolution.

In the oscillation code, the mesh points of the input stellar model are all taken into account. However, especially for oscillation modes with a large number of nodes, the mesh points in the stellar model may not be dense enough in regions where the wavelength is short, thus the difference in radius between two adjacent grids is much longer than the wavelength. This leads to the problem that the resolution is not enough to reveal the wave. Therefore, in the calculation of each oscillation mode, extra mesh points are temporarily added by linear interpolation to ensure that there are at least five mesh points in a wavelength, where the wavelength is estimated by using the dispersion relation.

3.5 Time Costs

The time cost for the YNEV code calculating stellar evolutionary models depends on the time/space step settings, stellar parameters (i.e. stellar mass), software (adopted Fortran compiler) and hardware. For a computer with two cores that have a ~ 3 GHz CPU and are compiled by using the Intel Fortran compiler, with the number of mesh points being 1000 \sim 1500 and the number of time grids \sim 1100, the process of YNEV evolving an intermediate-mass star from the PMS to the helium burning out in the core costs about five minutes. With the same time/space step settings, the process of YNEV evolving a low-mass star from the PMS to a low temperature white dwarf costs more than three hours, and the total number of time grids is about $\sim 30\,000$. The phase with the greatest time cost is the TP-AGB.

The part of the YNEV code with the greatest time cost is solving the nuclear reaction networks on all mesh point. The opacity and EOS are interpolated from tables with different metallicities because Z slightly changes in the hydrogen burning region. If we ignore this slight change and calculate opacity and EOS based on the tables with fixed Z , the time costs should be reduced. We have tested the time costs by using the nuclear reaction part of Paczyński's (1969) code to replace the nuclear reaction networks of YNEV and calculate opacity and EOS based on fixed Z . It is found that the time costs are significantly reduced, e.g. the case of an intermediate-mass star mentioned above costs only half a minute. In order to ensure accuracy, we usually prefer to use the nuclear reaction networks and interpolate opacity and EOS from tables with different metallicities.

The use of nonlocal TCM significantly increases time costs. The reason is that, for all stellar models in the evolutionary phases, the stellar structure equations and the TCM equations are solved alternately to find the final solution satisfying both equations. The case of an intermediate-mass star mentioned above costs nearly an hour when we adopt the nonlocal TCM to deal with stellar convection.

4 INITIAL MODEL

The YNEV code evolves a star from PMS with center temperature $T_C = 10^5$ K, zero age main sequence (ZAMS) or ZAHB. A database of initial PMS and ZAHB models with different stellar masses (both helium core mass and hydrogen envelope mass, for ZAHB models), metal compositions and fixed MLT parameter α in the cases of $X = 0.7$, $Z = 0.02$ and $X = 0.75$, $Z = 0$ are calculated offline and stored.

Table 1 Parameters of the Solar Models

Model	Z93	Z09	Z98OPKS	R98TCM
Atmosphere	EG	EG	KS	EG
Composition	GN93	AGSS09	GS98	GS98
Opacity	OPAL	OPAL	OP	OPAL
α	1.744	1.645	2.277	0.8069 (TCM)
X_0	0.7050	0.7179	0.7079	0.6998
Z_0	0.0201	0.0152	0.0189	0.0200
Y_s	0.2449	0.2359	0.2434	0.2565
Z_s	0.0181	0.0136	0.0170	0.0186
$(Z/X)_s$	0.0245	0.0181	0.0230	0.0257
R_{bc}/R_\odot	0.7136	0.7248	0.7140	0.7135
$[\text{Li}]/[\text{Li}]_0$	5.7%	14.8%	8.2%	1.7%

The initial PMS model for given input stellar parameters is obtained by reading a stored PMS model with the same metal composition and the closest stellar mass and using the method of Newton iterations to solve the stellar structure with required stellar parameters. Relaxations are automatically performed if there is no convergence in Newton iterations, i.e. the stellar parameters are gradually changed from the stored PMS model to the required values. The initial ZAHB model for the given input stellar parameters is obtained by using a similar method. For the ZAMS model, in order to ensure accuracy in the compositions of metals in the stellar interior (since they may change via nuclear burning in the PMS stage), we do not use offline calculated models. The adopted method to generate the ZAMS model evolves too quickly from PMS to ZAMS (defined by $X_S - X_C = 0.001$) by using half the number of mesh points and double the time steps.

5 SAMPLES OF STELLAR EVOLUTION AND OSCILLATIONS

5.1 Solar Models

We have used the YNEV code to calculate four solar models named Z93, Z09, Z98OPKS and R98TCM with different input physics. The models are evolved from ZAMS to the solar age of 4.57 Gyr. Their radii and luminosity are calibrated to $R_\odot = 6.96 \times 10^{10}$ cm and $L_\odot = 3.846 \times 10^{33}$ erg s⁻¹ with an accuracy of 10^{-4} . In model Z93, the OPAL opacity and Eddington gray (EG) model are used, the solar composition GN93 is adopted and the ratio of metallicity to hydrogen $(Z/X)_S$ is calibrated to be 0.0245 (Grevesse & Noels 1993). In model Z09, the OPAL opacity and EG model are used, the solar composition given by AGSS09 is adopted and $(Z/X)_S$ is calibrated to be 0.0181 which is also consistent with AGSS09.

In model Z98OPKS, the OP opacity and Krishna Swamy's (1966) atmosphere model (KS) are used, the solar composition GS98 is adopted and $(Z/X)_S$ is calibrated to be 0.023 (Grevesse & Sauval 1998). The MLT is applied in the Z93, Z09 and Z98OPKS models. In model R98TCM, the GS98 composition (Grevesse & Sauval 1998), the OPAL opacity and Eddington gray model are used, the TCM and the updated convective overshoot mixing model are adopted, and the base of the convective envelope is calibrated to be $R_{bc}/R_\odot = 0.7135$. Key information about the solar models is listed in Table 1. A comparison of sound speed between models and helioseismic inversions (Basu et al. 2009) are shown in Figure 1. Comparing with MESA (Paxton et al. 2011), the YNEV solar model Z98OPKS shows almost the same results for the same parameters, e.g. for MESA, $X_0 = 0.7065$, $Z_0 = 0.0191$, $Y_s = 0.2433$, $Z_s = 0.0170$, $R_{bc}/R_\odot = 0.7140$ and the differences in sound speed for MESA (see Paxton et al. 2011, fig. 21) are also similar to those given by YNEV.

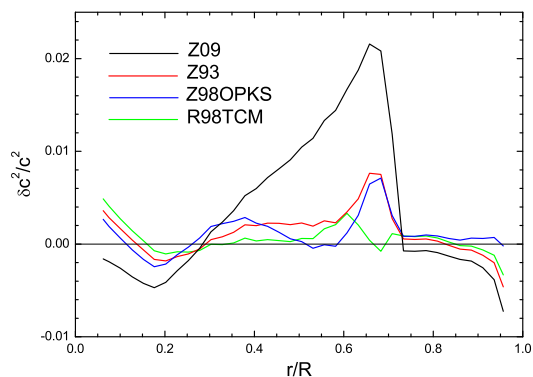


Fig. 1 Differences in sound speed between models and helioseismic inversions.

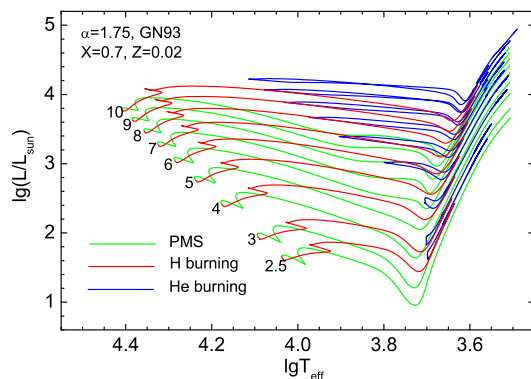


Fig. 2 Evolutionary tracks of intermediate-mass stars with $X = 0.7$, $Z = 0.02$ and MLT parameter $\alpha = 1.75$. The metal composition is the same as GN93. In the tracks, the green, red and blue parts correspond to PMS, hydrogen burning and helium burning phases respectively. The numbers near the ZAMSs indicate the stellar mass (in units of solar mass).

5.2 Evolutionary Tracks in the HR Diagram: for the Classical MLT Theory

Evolutionary tracks of intermediate-mass stars with mass between $2.5 \leq M/M_{\odot} \leq 10$ generated by the YNEV code are shown in Figures 2 and 3. The two figures show results for different stellar chemical compositions. Stars evolve from the PMS with $T_C = 10^5$ K to the asymptotic branch giant (AGB) stage. The PMS stage, the hydrogen burning stage (defined by $X_S - X_C \geq 0.001$ and $X_C + Y_C \geq 0.95$) and the helium burning stage (defined by $X_C + Y_C \leq 0.95$) are shown as green, red and blue lines, respectively. The YNEV evolutionary tracks are similar to tracks calculated by the FRANEC code. The blue loops for intermediate-mass stars are sensitive to results in stellar evolutionary codes. Comparing Figure 2 with the FRANEC evolutionary tracks (see Bono et al. 2000, fig. 3), it can be found that the tips of the blue loops in YNEV and FRANEC are at almost the same locations: ($\lg T \approx 4.12$, $\lg L \approx 4.2$) for a $10 M_{\odot}$ star, ($\lg T \approx 4.03$, $\lg L \approx 3.9$) for an $8 M_{\odot}$ star, ($\lg T \approx 3.97$, $\lg L \approx 3.65$) for a $7 M_{\odot}$ star, ($\lg T \approx 3.90$, $\lg L \approx 3.4$) for a $6 M_{\odot}$ star, and ($\lg T \approx 3.78$, $\lg L \approx 3.0$) for a $5 M_{\odot}$ star.

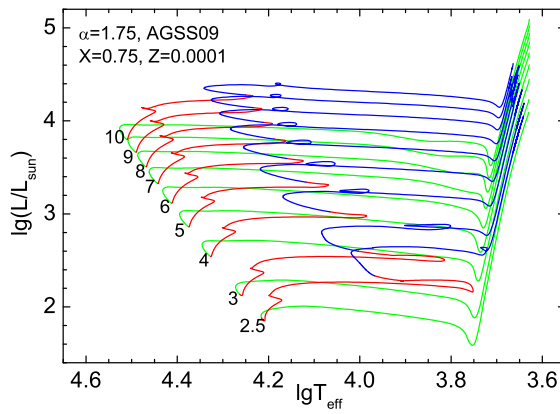


Fig. 3 Similar to Fig. 2, but for $X = 0.75$, $Z = 0.0001$ and the AGSS09 metal composition.

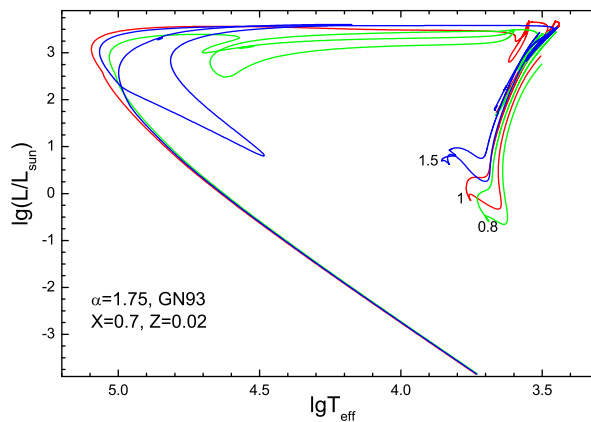


Fig. 4 Evolutionary tracks of $1.5 M_{\odot}$, $1 M_{\odot}$ and $0.8 M_{\odot}$ stars with $X = 0.7$, $Z = 0.02$ and MLT parameter $\alpha = 1.75$. The metal composition is the same as GN93.

Three samples of evolutionary tracks for low-mass stars from PMS to white dwarf phases are shown in Figure 4. When the helium flashes occur, the locations of the stars automatically jump to ZAHB without tracing the helium flash process in detail. After the end of center helium burning, Reimers's (1975) mass loss rate is adopted. For the $1.5 M_{\odot}$ star, the mass loss rate is enhanced by a factor of 5. The stars lose their envelope in the AGB stage and finally evolve to white dwarfs.

The YNEV evolution code traces variations in isotopes D and ${}^7\text{Li}$, thus one can use it to study the depletion of light elements D and ${}^7\text{Li}$ in the PMS stage. Figure 5 shows the evolutionary tracks of stars with $0.15 \leq M/M_{\odot} \leq 1$ from PMS to ZAMS and denotes the depletions (to 1% of initial abundance) of D and ${}^7\text{Li}$ at the stellar surface. Compared with the MESA code (see Paxton et al. 2011, fig. 15), the YNEV code shows similar results, since both YNEV and MESA yield the same luminosity for the of D and ${}^7\text{Li}$. The stellar models are standard in that only the full mixing occurs in the convectively unstable zone and there is no extra mixing.

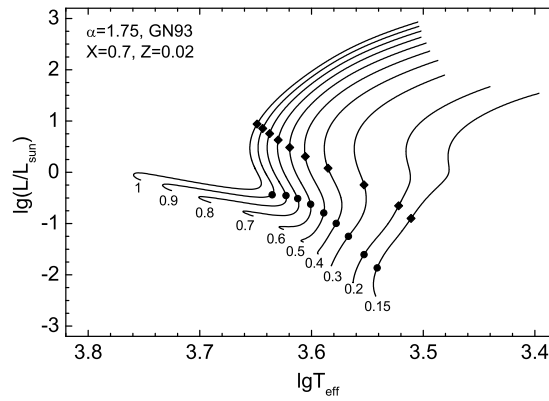


Fig. 5 Evolutionary tracks of stars with $0.15 \leq M/M_{\odot} \leq 1$ from PMS to ZAMS. $X = 0.7$, $Z = 0.02$ and MLT parameter $\alpha = 1.75$. The metal composition is the same as GN93. Diamonds and circles denote the location of $[D]/[D]_0 = 1\%$ and $[{}^7\text{Li}]/[{}^7\text{Li}]_0 = 1\%$ at the stellar surface. The number below each track shows the mass of the star (in solar masses).

5.3 Chemical Composition in the Stellar Interior: Comparison with the STAROX Code

Figures 6 and 7 show the compositions in the stellar interior of $0.9 M_{\odot}$ and $5 M_{\odot}$ stars with $X = 0.7$, $Z = 0.02$ at the stage $X_C = 0.35$. $\alpha = 1.75$ and the GN93 metal composition are used. The process of ${}^{12}\text{C}, {}^{16}\text{O} \rightarrow {}^{14}\text{N}$ in the CNO cycles are clearly shown. ${}^{16}\text{O} \rightarrow {}^{14}\text{N}$ can hardly occur in a $0.9 M_{\odot}$ star since the temperature in the core is low. Those examples are also shown by the STAROX stellar evolution code (Roxburgh 2008). Comparing the results from YNEV with those from STAROX, there is no significant difference except for the age of the $0.9 M_{\odot}$ star with $X_C = 0.35$, which is 6.839 Gyr in YNEV and 6.675 Gyr in STAROX. The difference is thought to be caused by the different initial abundance of isotopes in metals and ${}^3\text{He}$.

5.4 Evolutionary Tracks in the HR Diagram: for the Nonlocal Turbulent Convection Model

The most important feature of the YNEV code is the ability to use nonlocal turbulent convection theory in calculations of stellar structure and evolution. For example, we show the evolutionary tracks of low- and intermediate-mass stars in Figures (8)–(10). The value of the turbulent kinetic dissipation parameter α_{TCM} is based on the solar calibration, and the value of the overshoot mixing parameter C_{OV} is based on some observational restrictions (Zhang 2013; Meng & Zhang 2014). The stars evolve from the PMS with center temperature $T_C = 10^5$ K to where the numerical scheme cannot find a solution satisfying both the TCM and the stellar structure equations. The localized TCM is used in the PMS with $\lg T_C < 6.8$, and the nonlocal TCM is used after that. It can be found that the scheme implementing the nonlocal TCM works well in most cases of stellar evolution.

5.5 Comparing the Nonlocal Turbulent Convection YNEV Stellar Model with the Padova and Yale-Yonsei Models

Figures 11 and 12 show the evolutionary tracks computed with the Padova (Bressan et al. 1993; Salasnich et al. 2000; Girardi et al. 2000), Yale-Yonsei (Y^2) (Yi et al. 2001; Kim et al. 2002; Yi et al. 2003; Demarque et al. 2004) and YNEV stellar models. The nonlocal TCM and the updated overshoot mixing model are used in the YNEV models, with $\alpha_{\text{TCM}} = 0.8$ and $C_{\text{OV}} = 10^{-3}$. The

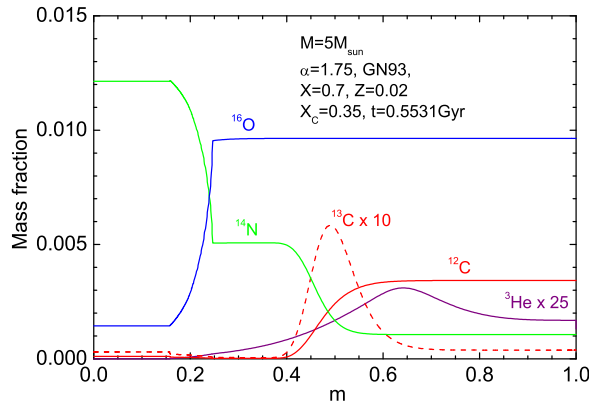


Fig. 6 Chemical composition in the stellar interior of a star with $M = 5 M_{\odot}$ and $X_C = 0.35$. $X = 0.7$, $Z = 0.02$ and MLT parameter $\alpha = 1.75$. The metal composition is the same as GN93.

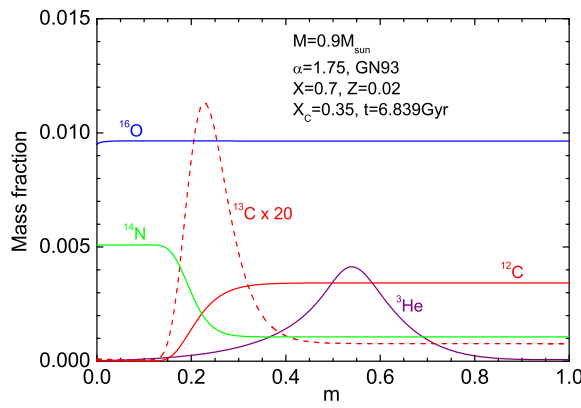


Fig. 7 Similar to Figure 6, but for a $0.9 M_{\odot}$ star.

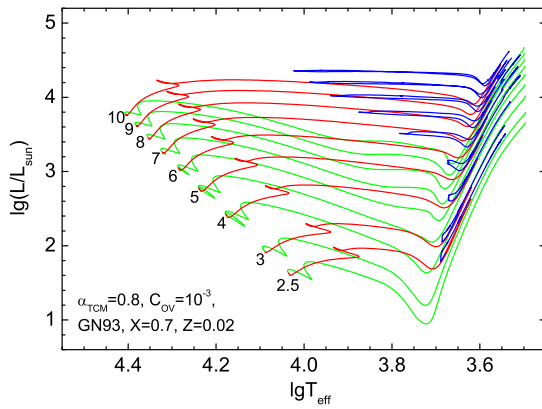


Fig. 8 Evolutionary tracks of an intermediate-mass stars with $X = 0.7$, $Z = 0.02$, the nonlocal turbulent convection model (convection parameter $\alpha_{\text{TCM}} = 0.8$) and the updated overshoot model (with $C_{\text{OV}} = 10^{-3}$). The metal composition is the same as GN93. In the tracks, the green, red and blue parts correspond to PMS, hydrogen burning and helium burning phases respectively. The numbers near the ZAMSs indicate the stellar mass (in units of solar mass).

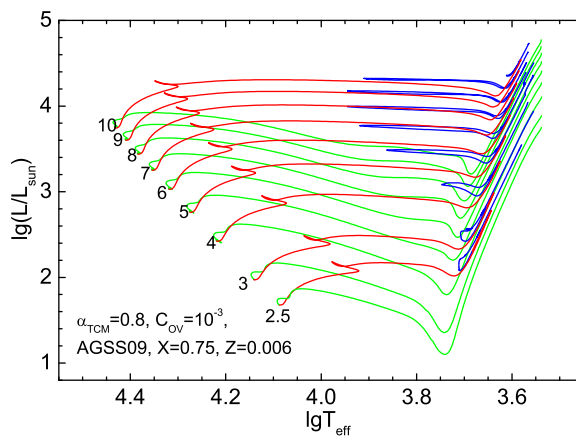


Fig. 9 Similar to Fig. 8, but for $X = 0.75$, $Z = 0.006$ and the AGSS09 composition.

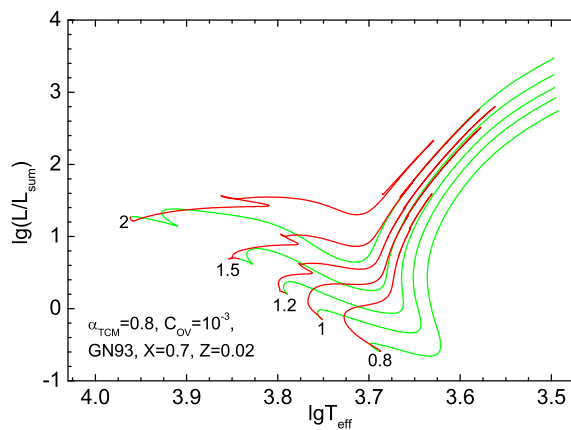


Fig. 10 Similar to Fig. 8, but for low-mass stars.

Padova stellar models have $X = 0.708$, $Z = 0.019$ and incorporate the ballistic overshoot model (Bressan et al. 1981) with an overshoot parameter that depends on stellar mass. The Y^2 stellar models have $X = 0.71$, $Z = 0.02$ and utilize a fully mixed core overshoot region in $\alpha_{OV} H_P$ with the overshoot parameter α_{OV} depending on stellar mass (Demarque et al. 2004).

Table 2 shows the age of the critical points in the stellar evolutionary tracks computed with the Padova, Y^2 and YNEV (with nonlocal TCM) models. It is found that the age of the critical points in the YNEV stellar models with nonlocal TCM and the updated overshoot is the same as Padova and Y^2 , except for the main sequence (MS) age of the low-mass star. The MS age for the YNEV stellar models is a little larger than that of Padova and Y^2 . Those results show that the core overshoot mixing strength in the three codes is similar and, for a low-mass star, YNEV shows slightly stronger overshoot mixing. It can be noticed that the overshoot parameters in Padova and Y^2 depend on stellar mass but the overshoot parameter in the YNEV is constant.

Figure 11 shows the tracks for intermediate-mass stars. The widths of the main sequence band for the three models indicate that the strengths of core overshoot mixing in the three codes are similar.

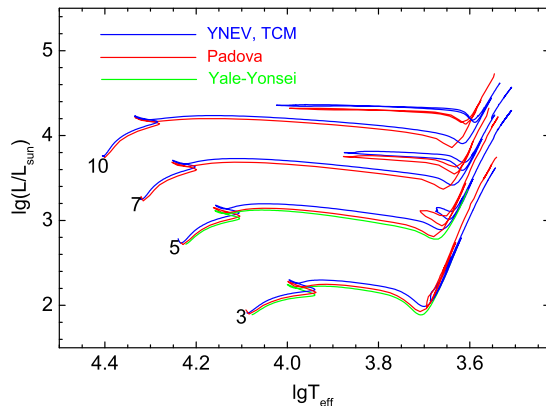


Fig. 11 Evolutionary tracks computed with the Padova, Yale-Yonsei and YNEV models for intermediate mass stars. The results from the YNEV model are the same those shown in Fig. 10.

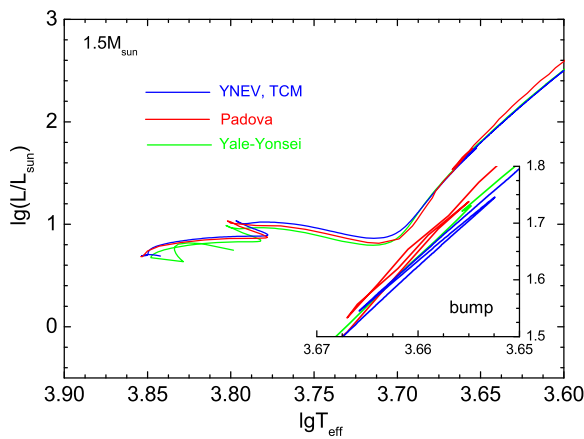


Fig. 12 Similar to Fig. 11, but for a $1.5 M_{\odot}$ star. The area around the bump is enlarged.

The extensions of the blue loops in the results from YNEV and Padova are similar. Compared to the Padova tracks, the YNEV tracks have a lower temperature in the red giant branch (RGB) phase and the differences increase as the stellar mass increases. It should be noticed that the low-temperature opacity table in YNEV is different from that in Padova, i.e. Ferguson et al.'s (2005) tables are adopted in YNEV and Alexander & Ferguson's (1994) tables are adopted in Padova. The efficiency of the turbulent heat transport in the super-adiabatic convection zone shows a difference between the TCM and the MLT.

Figure 12 shows the case of a $1.5 M_{\odot}$ star. The main difference is that the YNEV and Padova models show a large bump in the RGB phase, but the Y^2 model shows a small bump. We think that this is caused by the absence of the overshoot mixing below the convective envelope in the Y^2 model.

5.6 Stellar Oscillations

The linear adiabatic oscillation part of the YNEV code is designed to scan the eigenfrequencies and solve the eigenfunctions of stellar adiabatic oscillations. Here we show two examples of applications

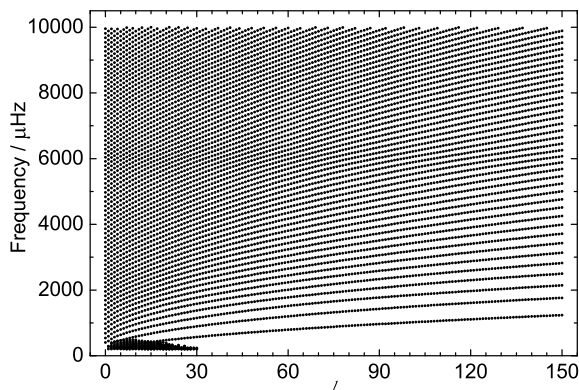


Fig. 13 Eigenfrequencies in the range $200 \leq f/\mu\text{Hz} \leq 10\,000$ of the solar model Z93 for $0 \leq l \leq 150$.

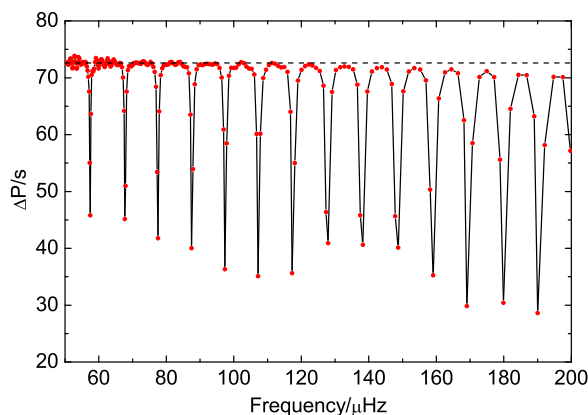


Fig. 14 Relation between period spacing and frequency of a $1.5 M_{\odot}$ RGB star with $R = 6.38 R_{\odot}$ and $L = 19.3 L_{\odot}$. The dashed line shows the asymptotic value $\Delta P = 72.61\text{s}$.

of the YNEV oscillation code: oscillations in the solar model and mixed modes in an RGB low-mass star.

Figure 13 shows the eigenfrequencies of the solar model Z93 calculated by using the YNEV oscillation code. The eigenfrequencies are in the range $200 \leq f/\mu\text{Hz} \leq 10\,000$ for $0 \leq l \leq 150$. The dense part represents low frequencies with low l that are g-modes and the other parts are p-modes. Figure 14 shows the relation between period spacing ΔP and frequency f of the $1.5 M_{\odot}$ RGB star with radius $R = 6.38 R_{\odot}$ and luminosity $L = 19.3 L_{\odot}$. A similar example was studied by Bedding et al. (2011) using the ASTEC evolution code (Christensen-Dalsgaard 2008a) and the ADIPLS oscillation code (Christensen-Dalsgaard 2008b).

6 DEVELOPMENTS PLANNED FOR THE FUTURE

There are many ways in which the code could be improved. In order to calculate results for massive stars, more nuclear burning reactions should be included, and a possible H-semiconvection zone and convective burning shell(s) outside the convective core should be treated properly. At present, the

Table 2 The age (in Gyr) of critical points in stellar evolution. (Y2), (P) and (YN) mean Yale-Yonsei, Padova and YNEV models, respectively.

Critical point	$1.5 M_{\odot}$	$3 M_{\odot}$	$5 M_{\odot}$	$7 M_{\odot}$	$10 M_{\odot}$
H burned out in the center	2.895 (Y2)	0.3921 (Y2)	0.1040 (Y2)	- (Y2)	- (Y2)
	2.755 (P)	0.3793 (P)	0.1031 (P)	0.04784 (P)	0.02379 (P)
	3.175 (YN)	0.3855 (YN)	0.1023 (YN)	0.04735 (YN)	0.02350 (YN)
He ignition in the center	- (Y2)	- (Y2)	- (Y2)	- (Y2)	- (Y2)
	- (P)	0.3834 (P)	0.1037 (P)	0.04803 (P)	0.02384 (P)
	- (YN)	0.3905 (YN)	0.1031 (YN)	0.04759 (YN)	0.02357 (YN)
He burned out in the center	- (Y2)	- (Y2)	- (Y2)	- (Y2)	- (Y2)
	- (P)	0.4763 (P)	0.1174 (P)	0.05277 (P)	0.02585 (P)
	- (YN)	0.4775 (YN)	0.1167 (YN)	0.05293 (YN)	0.02608 (YN)

stellar structure and composition are solved individually. A better approach is to solve them together. The two point second order discretization could be upgraded to a higher order scheme. An important improvement would be to apply parallel numerical calculations, which could significantly boost the calculation speed. To my knowledge, YNEV is the first stellar evolution code that can incorporate a nonlocal turbulent convection model in most simulations of stellar evolution. As mentioned above, there are still some numerical problems when implementing the nonlocal TCM. Correcting those numerical problems is a priority. There is no doubt that the reader can think of other ways in which the code could be improved.

Acknowledgements QSZ thanks a referee for their constructive comments which improved the original manuscript. This work is co-sponsored by the National Natural Science Foundation of China through (Grant No. 11303087), the West Light Foundation of the Chinese Academy of Sciences, the Science Foundation of Yunnan Observatories (Grant Nos. Y1ZX011007 & Y3CZ051005) and the Chinese Academy of Sciences (Grant No. KJCX2-YW-T24). Fruitful discussions with Yan Li and Jørgen Christensen-Dalsgaard are highly appreciated.

References

- Alexander, D. R., & Ferguson, J. W. 1994, *ApJ*, 437, 879
Angulo, C., Arnould, M., Rayet, M., et al. 1999, *Nuclear Physics A*, 656, 3
Aparicio, J. M. 1998, *ApJS*, 117, 627
Asplund, M., Grevesse, N., Sauval, A. J., & Scott, P. 2009, *ARA&A*, 47, 481
Basu, S., Chaplin, W. J., Elsworth, Y., New, R., & Serenelli, A. M. 2009, *ApJ*, 699, 1403
Bedding, T. R., Mosser, B., Huber, D., et al. 2011, *Nature*, 471, 608
Böhm-Vitense, E. 1958, *ZAp*, 46, 108
Bono, G., Caputo, F., Cassisi, S., et al. 2000, *ApJ*, 543, 955
Bressan, A. G., Chiosi, C., & Bertelli, G. 1981, *A&A*, 102, 25
Bressan, A., Fagotto, F., Bertelli, G., & Chiosi, C. 1993, *A&AS*, 100, 647
Canuto, V. M. 1997, *ApJ*, 482, 827
Canuto, V. M., & Dubovikov, M. 1998, *ApJ*, 493, 834
Canuto, V. M. 2011, *A&A*, 528, A76
Cassisi, S., Potekhin, A. Y., Pietrinferni, A., Catelan, M., & Salaris, M. 2007, *ApJ*, 661, 1094
Castellani, V., Chieffi, A., Tornambe, A., & Pulone, L. 1985, *ApJ*, 296, 204
Caughlan, G. R., & Fowler, W. A. 1988, *Atomic Data and Nuclear Data Tables*, 40, 283
Christensen-Dalsgaard, J. 2008a, *Ap&SS*, 316, 13
Christensen-Dalsgaard, J. 2008b, *Ap&SS*, 316, 113
Christensen-Dalsgaard, J., Monteiro, M. J. P. F. G., Rempel, M., & Thompson, M. J. 2011, *MNRAS*, 414, 1158

- de Jager, C., Nieuwenhuijzen, H., & van der Hucht, K. A. 1988, *A&AS*, 72, 259
- Demarque, P., Woo, J.-H., Kim, Y.-C., & Yi, S. K. 2004, *ApJS*, 155, 667
- Deng, L., Xiong, D. R., & Chan, K. L. 2006, *ApJ*, 643, 426
- Dewitt, H. E., Graboske, H. C., & Cooper, M. S. 1973, *ApJ*, 181, 439
- Ferguson, J. W., Alexander, D. R., Allard, F., et al. 2005, *ApJ*, 623, 585
- Girardi, L., Bressan, A., Bertelli, G., & Chiosi, C. 2000, *A&AS*, 141, 371
- Grevesse, N., & Noels, A. 1993, in *Origin and Evolution of the Elements*, eds. N. Prantzos, E. Vangioni-Flam, & M. Casse (Cambridge: Cambridge Univ. Press), 15
- Grevesse, N., & Sauval, A. J. 1998, *Space Sci. Rev.*, 85, 161
- Iben, I., Jr. 1975, *ApJ*, 196, 525
- Iglesias, C. A., & Rogers, F. J. 1996, *ApJ*, 464, 943
- Itoh, N., Hayashi, H., Nishikawa, A., & Kohyama, Y. 1996, *ApJS*, 102, 411
- Kim, Y.-C., Demarque, P., Yi, S. K., & Alexander, D. R. 2002, *ApJS*, 143, 499
- Krishna Swamy, K. S. 1966, *ApJ*, 145, 174
- Li, Y., & Yang, J. Y. 2007, *MNRAS*, 375, 388
- Li, Y. 2012, *ApJ*, 756, 37
- Meng, Y., & Zhang, Q. S. 2014, *ApJ*, 787, 127
- Paczyński, B. 1969, *Acta Astronomica*, 19, 1
- Paxton, B., Bildsten, L., Dotter, A., et al. 2011, *ApJS*, 192, 3
- Reimers, D. 1975, *Memoires of the Societe Royale des Sciences de Liege*, 8, 369
- Rogers, F. J., & Nayfonov, A. 2002, *ApJ*, 576, 1064
- Roxburgh, I. W. 2008, *Ap&SS*, 316, 75
- Salasnich, B., Girardi, L., Weiss, A., & Chiosi, C. 2000, *A&A*, 361, 1023
- Salpeter, E. E. 1954, *Australian Journal of Physics*, 7, 373
- Seaton, M. J. 2005, *MNRAS*, 362, L1
- Thoul, A. A., Bahcall, J. N., & Loeb, A. 1994, *ApJ*, 421, 828
- Timmes, F. X., & Arnett, D. 1999, *ApJS*, 125, 277
- Waldron, W. L. 1985, *NASA Conference Publication*, 2358, in *The Origin of Non-Radiative Heating/Momentum in Hot Stars*, eds. A. B. Underhill & A. G. Michalitsianos, 95
- Xiong, D. 1981, *Scientia Sinica*, 24, 1406
- Xiong, D. R., Cheng, Q. L., & Deng, L. 1997, *ApJS*, 108, 529
- Yakovlev, D. G., & Urpin, V. A. 1980, *Soviet Ast.*, 24, 303
- Yi, S., Demarque, P., Kim, Y.-C., et al. 2001, *ApJS*, 136, 417
- Yi, S. K., Kim, Y.-C., & Demarque, P. 2003, *ApJS*, 144, 259
- Zhang, Q. S. 2012, *ApJ*, 761, 153
- Zhang, Q. S. 2013, *ApJS*, 205, 18
- Zhang, Q. S. 2014, *ApJ*, 787, L28
- Zhang, Q. S., & Li, Y. 2012, *ApJ*, 746, 50